OPEN

International Journal of Oral Science (2017) 9, 87–94
www.nature.com/ijos

ORIGINAL ARTICLE

A robust methodology for the quantitative assessment of the rat jawbone microstructure

Marissa Chatterjee[1], Fernanda Faot[1,2], Cassia Correa[1,3], Joke Duyck[1], Ignace Naert[1] and Katleen Vandamme[1]

Micro-computed tomography can be applied for the assessment of the micro-architectural characteristics of the cortical and trabecular bones in either physiological or disease conditions. However, reports often lack a detailed description of the methodological steps used to analyse these images, such as the volumes of interest, the algorithms used for image filtration, the approach used for image segmentation, and the bone parameters quantified, thereby making it difficult to compare or reproduce the studies. This study addresses this critical need and aims to provide standardized assessment and consistent parameter reporting related to quantitative jawbone image analysis. Various regions of the rat jawbones were screened for their potential for standardized micro-computed tomography analysis. Furthermore, the volumes of interest that were anticipated to be most susceptible to bone structural changes in response to experimental interventions were defined. In the mandible, two volumes of interest were selected, namely, the condyle and the trabecular bone surrounding the three molars. In the maxilla, the maxillary tuberosity region and the inter-radicular septum of the second molar were considered as volumes of interest. The presented protocol provides a standardized and reproducible methodology for the analysis of relevant jawbone volumes of interest and is intended to ensure global, accurate, and consistent reporting of its morphometry. Furthermore, the proposed methodology has potential, as a variety of rodent animal models would benefit from its implementation.
International Journal of Oral Science (2017) **9,** 87–94; doi:10.1038/ijos.2017.11; published online 16 June 2017

Keywords: bone microarchitecture; jawbone; methodology; micro-computed tomography; rat

INTRODUCTION

Conventionally, quantitative histology is the standard technique for assessing the trabecular and cortical bone architecture. Although histology yields conclusive information on cellularity and tissue in a specific analysed volume, it has limitations with regard to the assessment of the bone microarchitecture because all of the structural parameters are from the stereological analysis of two-dimensional (2D) sections, assuming that the structure is usually plate like.[1–2] Moreover, high-cost and labour-intensive analysis has brought about the need for the development of imaging techniques that can overcome the disadvantages posed by histology.[3] In this context, the appearance of micro-computed tomography (micro-CT) has made it possible for clinicians and researchers to analyse the three-dimensional (3D) structure of bone, both in human biopsies and experimental models.[4–5] Furthermore, micro-CT enables the direct measurement of the bone microarchitecture without depending on stereological models. This advanced micro-imaging method is now being widely used to determine the volume of bone mass and the microarchitecture indices of native and newly formed bone by means of morphometric parameters (2D and 3D) and mineral density.[1,6] Introduced in the late 1980s by Feldkamp *et al.*,[7] micro-CT has now become the "gold standard" for estimating bone morphology and microstructure in mice and other small animal models *ex vivo* and *in vivo*.

By enabling the quantitative assessment of the bone's macrostructural and microstructural characteristics, such as geometry, bone volume (BV), bone thickness, and connectivity, micro-CT improves our ability to estimate the quality of bone.[8] However, for animal experiments, the outcome varies and more often than not depends on the experimental rationale and the applied protocol. With regard to the jawbones, micro-CT has been widely used to study alveolar bone remodelling,[8–10] dynamic changes that occur in the periodontal ligament thickness,[11] and specific osseous sites in both the cortical and trabecular compartments.[12–18] However, related to protocols for rodent jawbones (maxilla and mandible), the literature is particularly scarce and the methodology for a comprehensive and reproducible quantitative analysis is not informative or detailed enough. Only one report published by Kallai *et al.*[8] has detailed the steps for micro-CT analysis in a mouse model. However, focus was given to the following three specific models of bone tissue regeneration: ectopic bone formation model, segmental defect in a long bone model, and critical-size mandibular bone defect model. Furthermore, Bagi *et al.*[14] evaluated the cortical and cancellous bone parameters for the

[1]Department of Oral Health Sciences & Dental Clinic, Biomaterials—BIOMAT, KU Leuven & University Hospitals Leuven, Leuven, Belgium; [2]Federal University of Pelotas—School of Dentistry, Pelotas, Brazil and [3]University of Campinas—UNICAMP/Piracicaba Dental School, Piracicaba, Brazil
Correspondence: Professor K Vandamme, Department of Oral Health Sciences & Dental Clinic, Biomaterials—BIOMAT, KU Leuven & University Hospitals Leuven, Kapucijnenvoer 7 Blok A Box 7001, Leuven BE-3000, Belgium
E-mail: Katleen.Vandamme@kuleuven.be
Accepted 14 February 2017

mandible in different animal models (mice, rats, rabbits, dogs, and nonhuman primates) using micro-CT imaging. In addition to the above-mentioned papers, other animal studies have described morphological measurements by micro-CT in rodent jawbones under varied conditions, including the evaluation of the effect of mechanical loading and of the hormonal status, such as osteoporosis[12,19] and diabetes,[20] on the bone morphology.

When attempting to compare the trabecular structure of jawbones among different rodent species in the anatomical areas of the jawbone surrounding the molars, it was found that these areas are challenging to quantify, as the trabecular bone is less homogenous than that seen in long bones.[21] This has highlighted important methodological challenges that need to be addressed.[22] One of the issues deals with the size of the volume of interest (VOI). Trabecular structure and number are site-dependent; thus, it is important to note that the size of the VOI should be such that the trabeculae included in the VOI are connected primarily to other trabeculae and do not connect to cortical bone. In rodent species, this should be taken care of primarily as the size of the VOI is comparatively smaller than other species. The second issue concerns the use of a standardized VOI. Equally sized VOIs applied to the images of different samples are critical in avoiding biased results. Indeed, the study by Lazenby *et al.*[23] suggest that changes in trabecular parameters were observed when using inappropriately sized VOIs; the outcome of the parameters' trabecular connectivity and structure appeared to be particularly sensitive to changes in the VOI size. The third issue is the variation in the VOI positioning within the jawbone to be analysed. As observed by Whitehouse *et al.*,[24] the percentage of BV varied between 12% and 37% depending on the position of the VOI, and even a slight shift (that is, a few micrometres) can result in a change of 1%–13% in the BV value. Therefore, it is crucial to identify appropriate VOI locations in determining anatomically homogenous VOIs across the specimens for meaningful comparisons of the bone microarchitecture. This is particularly true when analysing the trabecular structure of bones with a complex anatomy, such as the jawbone and its teeth. Moreover, many of the studies that have applied micro-CT analysis for rodent jawbones are lacking details on the methodological procedure and parameters adopted. Thus, it has become impossible to directly compare the qualitative and quantitative results of the rodent jawbone microarchitecture with regard to bone type evaluated, volumes of interest selected, algorithms used for image filtration, the approach used for image segmentation, and the measurement of the outcome variables.

Therefore, the objective of this methodological paper is to provide a detailed protocol for reproducible quantitative analysis by micro-CT of the rat mandible and maxilla. We examined the trabecular structure in four anatomical areas of the jawbone, namely, the condyle, the alveolar bone surrounding the molars in the mandible, the alveolar bone surrounding the second molar in the maxilla, and the tuberosity region of the maxilla. For this analysis, we used both manual and semi-automatic delineation of different regions of interest (ROIs) composing the VOI. We addressed methodological issues concerning the positioning of the ROI by using well-defined landmarks as references, image filtration, and image segmentation algorithms, along with robust and reproducible quantification of the trabecular structure of the rat jawbone.

MATERIALS AND METHODS

Animal experiments

According to the ARRIVE guidelines for the reporting of animal experiments,[25–26] all experimental protocols were approved by the ethical committee of KU Leuven (P130/2010). To describe a new methodology to extract and quantify the trabecular bone structure in the rat jawbone using micro-CT imaging, a total of 16 female adult Wistar rats at 12 weeks of age were used. Animals were fed a standard laboratory diet (or chow) comprising 0.7% phosphorous and 1% calcium (SSNIFF, Soest, Germany) and tap water.

Specimen preparation

The animals were killed by cervical displacement under isoflurane-induced anaesthesia. The jawbones were excised. The mandible and maxilla were split into two symmetrical parts (hemi-mandible and hemi-maxilla) and fixated in 10% $CaCO_3$-buffered formalin solution (pH 7.4) at 4 °C for 48 h. They were further kept in 70% ethanol at 4 °C until the day of micro-CT scanning.

Micro-computed tomographic imaging

This protocol was designed for use with Skyscan 1172, a high-resolution micro-CT scanner (Bruker, Kontich, Belgium). While scanning, the right hemi-maxilla or hemi-mandible was placed in a polyethylene tube fixed onto a support by means of soft modelling clay. The samples were scanned along the sagittal plane from the condyle all the way to the molars, excluding the mandibular incisors, and from the dorsal tuberosity to the molars, excluding the maxillary incisors. The scanning parameters were 7.8 μm pixel size, 50 kV X-ray voltage, 200 μA electric current, and 0.5 mm Al filter. The data sets were reconstructed with NRecon software (SkyScan, Aartselaar, Belgium). Beam hardening and ring reduction were applied. The evaluation of the 2D-scanned data was handled by the software provided with the scanner: Data viewer and CtAn (Image Processing Language). The images were further segmented into binary images using a Gaussian filter and a fixed threshold (lower and upper grey threshold values of 70 and 224, respectively) in order to extract the mineralized tissues. The protocol was set up for micro-CT image analysis using Skyscan micro-CT software version 1.13. Adjustments may be needed if another company's software is used.

Definition of jawbone ROIs

The ROIs of the rat jawbone were selected based on their potential to be susceptible to bone structural changes in response to experimental interventions and because they enable robust and reproducible quantification of the trabecular bone. For the maxilla, the following ROIs were selected: (i) the inter-radicular septum of the second molar (Max. ROI. M2) and (ii) the tuberosity region (Max. ROI. Tub). These regions were selected mainly because of ease of visualization of the tooth root when compared to the first molar. The first molar is quite large and possesses five roots; the third molar is the smallest, leaving too small of a volume of bone to quantify. For the aforementioned reasons, the trabecular bone surrounding the second molar was chosen as one of the ROIs of the maxilla. The maxillary tuberosity (Max. ROI. Tub) is composed mostly of trabecular bone and is the load-bearing region due to mastication. Therefore, it is interesting to observe changes in the microstructure of the bone in these two regions of the maxilla. The ROIs quantified in the mandible included: (i) the bone surrounding the molar region for each individual molar (M1, M2, and M3) and (ii) the mandibular condylar head (Mand. ROI. Cond). For the bone surrounding the individual molars in the mandible, both semi-automatic and manual delineation of the ROIs was applied. For M1, three ROIs were defined: (i) manual ROI (Mand. ROI. M1), (ii) standardized ellipsoid ROI containing the trabecular bone close to the lingual surface of the mandible (Mand. ROI. M1. Lingual) and (iii) standardized ellipsoid ROI covering the trabecular

bone region close to the buccal surface of the mandible (Mand. ROI. M1. Buccal).The ROIs for M2 were (i) manual ROI (Mand. ROI. M2) and ellipsoid ROI for the inter-radicular septum of the roots of the molar (Mand. ROI. M2. InterRad). For M3, there was only one ROI selected, namely, (i) ellipsoid ROI for the inter-radicular septum of the roots of the molar (Mand. ROI. M3. InterRad) (Table 1). The rationale for selecting these mandibular ROIs is that compared to the maxilla, the mandible is more susceptible to microstructural changes (for example, in response to ovariectomy) in rodents[27–31] due to its simpler geometry than the maxilla, which is characterized by irregular and more complicated roots and the presence of the nasal and sinus cavities. Therefore, unlike the ROIs measured in the maxilla, the entire molar region of the mandible was taken into consideration. By doing so, this also provides insight into which among the three molars experience the most bone structural changes in response to ovariectomy. This in turn leads to the second ROI, measured in the condyle, which is the load-bearing region in the mandible. Depending on the bone structural changes in the molar region, it can collectively alter the load-bearing pattern in the mandibular condylar head, thereby leading to bone microstructural changes that should be quantified.

Table 1 ROIs

ROI	Abbreviation
Maxilla	
Inter-radicular septum of molar 2	Max. ROI. M2
Maxillary Tuber	Max. ROI. Tub
Mandible	
Manual ROI of molar X	Mand. ROI. M1/Mand. ROI. M2
Ellipsoid ROI close to the lingual surface	Mand. ROI. M1. Lingual
Ellipsoid ROI close to the buccal surface	Mand. ROI. M1. Buccal
Inter-radicular septum of molar 2	Mand. ROI. M2. InterRad
Inter-radicular septum of molar 3	Mand. ROI. M3. InterRad
Mandibular condylar head	Mand. ROI. Cond

ROI, regions of interest.

Analysis of the maxilla

The first VOI analysed was the volume covering the trabecular bone within the inter-radicular septum of the distal roots of the second maxillary molar (Max. ROI. M2) (Figure 1a, a1 and a2).To do so, a data set containing exclusively the second molar region was created by defining the top slice (that is, the slice where the crown of M2 first appears) and the bottom slice (the slice where the crown of M3 first appears). This data set contained an average of 280–350 slices. Using the Data Viewer software (Bruker, Kontich, Belgium), the sample was subsequently re-oriented and positioned in such way that the occlusal surface of the maxillary molar was facing upwards. Further on, the trans-axial data set was used for analysis, as this plane provides optimal visualization of the M2 anatomy. The analysis started by determining a reference point, which in this case was the middle slice of the data set. The drawing of the ROI was performed on 50 slices downwards from the reference point. For each slice within the defined VOI, the ROI was delineated by manually matching with the area occupied by the trabecular bone (region with porosities and voids) by freehand drawing. The ROIs were then interpolated for all slices (Figure 2a, a1 and a2).

The second maxillary VOI was the tuberosity region (Max. ROI. Tub) (Figure 1b, b1 and b2). As mentioned above, a subset of images containing exclusively the maxillary tuberosity was first created. The region started at the level where the tooth roots of M3 disappeared. The total number of slices analysed were 50 slices downwards from the top slice. Using Data Viewer, the sample was then re-oriented such that the tuberosity facing the maxillary sinus was oriented downwards. The trans-axial plane was used for the actual analysis. With the maxillary tuberosity visualized as a triangle with the base facing the maxillary sinus and the vertex facing the buccal surface, a standard ellipsoid area measuring 0.6 mm× 0.7 mm was positioned on each slice at a distance of 0.4 mm vertically from the vertex of the tuberosity. The ROIs were then interpolated for all slices. In this way, the ellipsoid area delineated and quantified the trabecular bone within this region (Figure 2b, b1 and b2).

Analysis of the mandible

For the analysis of the trabecular bone in the mandibular first molar region, a subset of slices containing only M1 data was created by

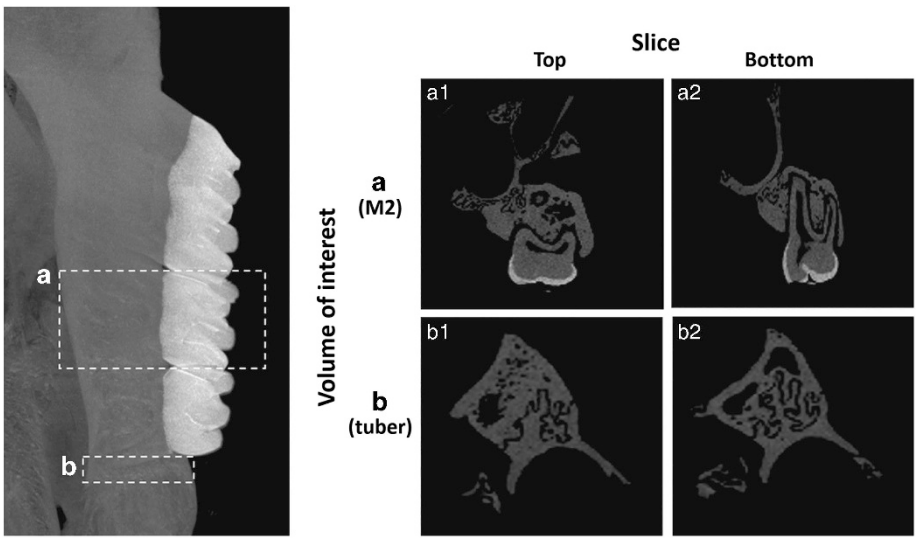

Figure 1 Micro-CT of the rat maxilla showing the selected volume of interest (VOI) data sets. (**a**) Definition of the top (**a**1) and bottom (**a**2) slices of the second maxillary molar in CtAn. (**b**) Definition of the top (**b**1) and bottom (**b**2) slices (100 slices) of the maxillary tuberosity in CtAn.

defining the top (that is, the slice where the crown of M2 first appears) and bottom slice (that is, the slice where the crown of M1 disappears). The data set contained an average of 370–400 slices. The reference slice selected was the middle slice of the data set containing M1 (Figure 3a, a1 and a2). The VOI defined for analysis was set at 100 slices downwards from the reference point. A total of 50 slices was investigated. On each of these slices, the ROI was delineated manually by freehand drawing (Mand. ROI. M1) (Figure 4a, a1) as well as *via* ellipsoid areas with standard dimensions (0.9 mm × 0.5 mm) positioned 0.6 mm horizontally from the midpoint of the incisor (Mand. ROI. M1. Lingual) and 1.0 mm vertically from the midpoint of the incisor (Mand. ROI. M1. Buccal), respectively (Figure 4a, a2 and a3).

In the same manner, for the analysis of M2, the subset was created containing solely the M2 region by defining the top (that is, the slice where the crown of molar three appears) and bottom slice (that is, the slice where the crown of M2 appears). The data set on average

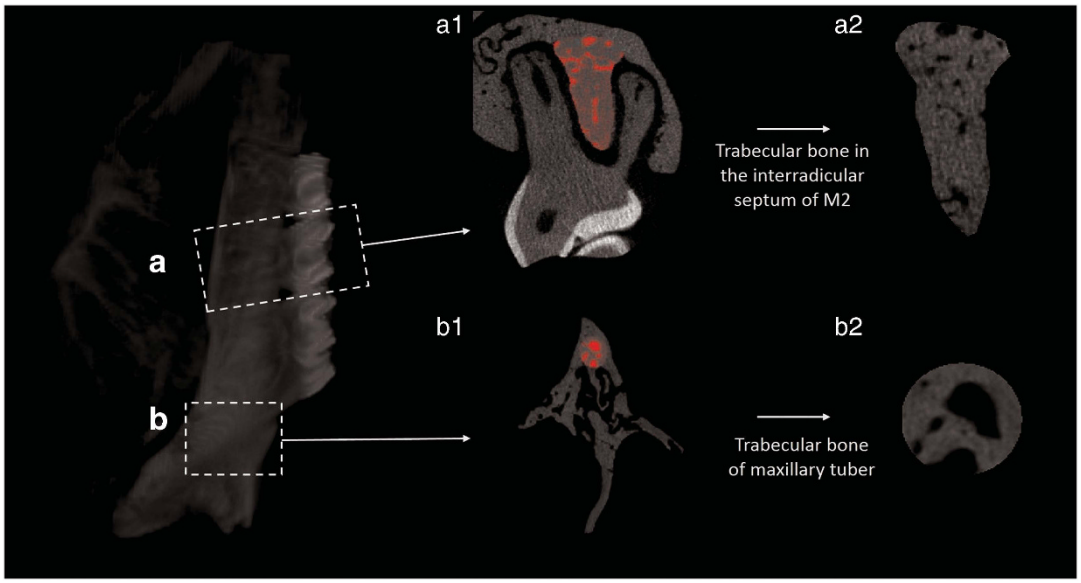

Figure 2 Micro-CT of the rat maxilla showing the selected ROI. (**a**: **a**1, **a**2) Inter-radicular septum of M2 (manually drawn ROI delineating the trabecular bone). (**b**: **b**1, **b**2) Tuberosity (ellipsoid-shaped ROI). M, molar teeth; ROI, region of interest.

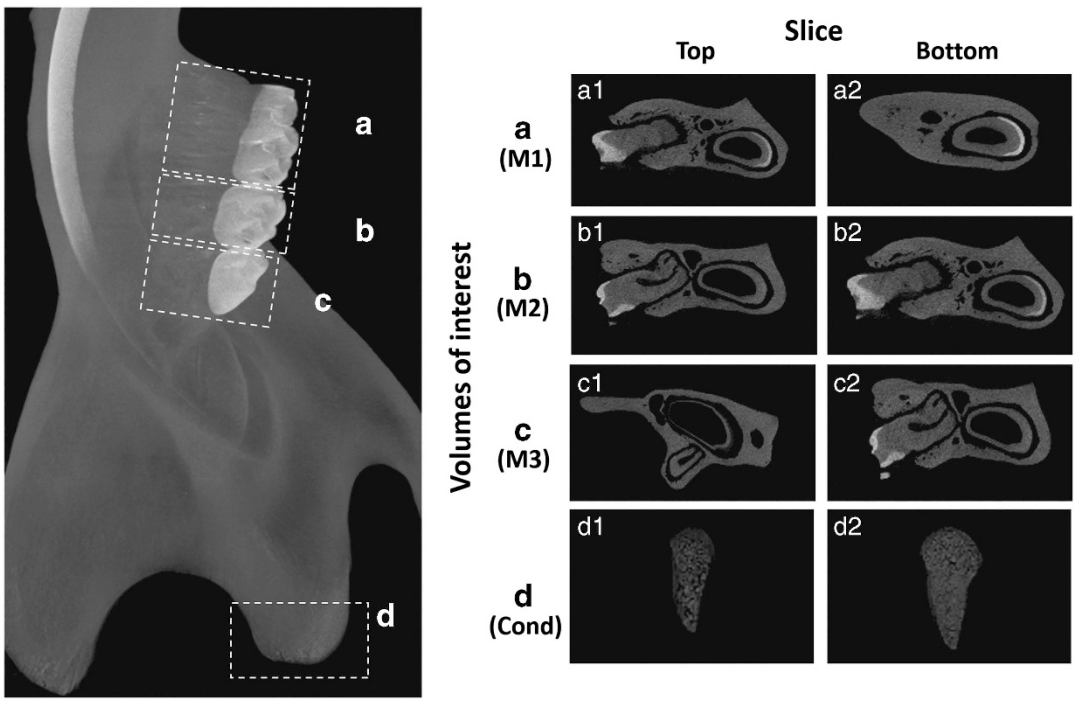

Figure 3 Micro-CT of the rat mandible showing the selected VOI data sets. (**a**) Definition of the top (**a**1) and bottom (**a**2) slices of M1 in CtAn. (**b**) Definition of the top (**b**1) and bottom (**b**2) slices of M2 in CtAn. (**c**) Definition of the top (**c**1) and bottom (**c**2) slices of M3 in CtAn. (**d**: **d**1, **d**2) VOI measured in the condyle (cond) using CtAn. Cond, condyle; M, molar teeth; VOI, volume of interest.

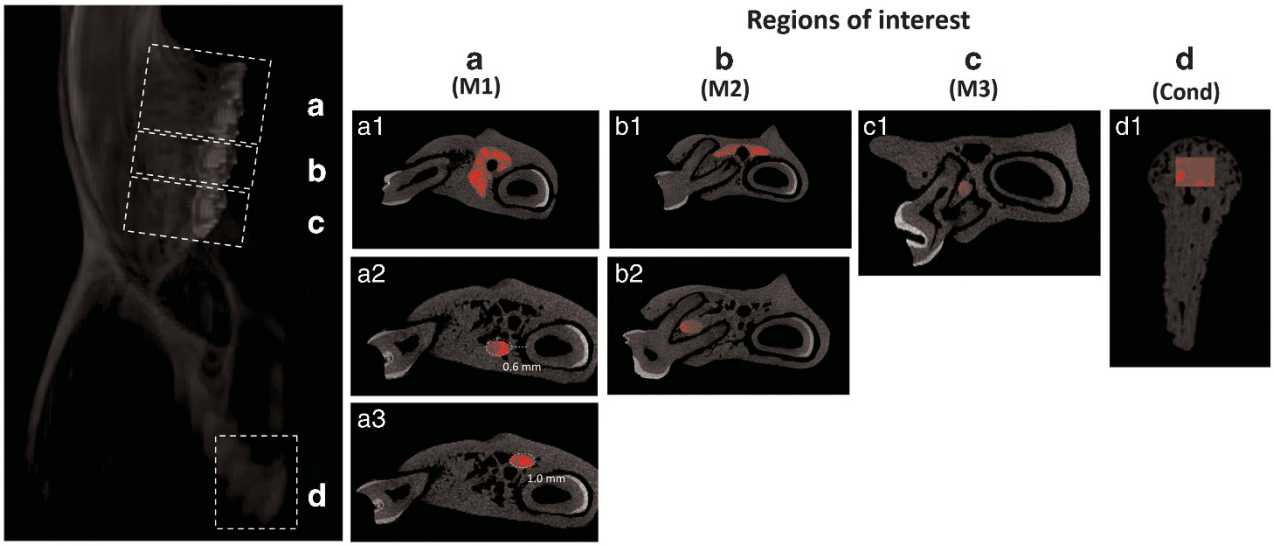

Figure 4 Micro-CT of the rat mandible showing the selected ROI. (**a**, **a**1) Trabecular bone of M1 (manually drawn ROI delineating the trabecular bone). (**a**, **a**2) Trabecular bone of M1 close to the lingual surface (standard ellipsoid-shaped ROI). (**a**, **a**3) Trabecular bone of M1 close to the buccal surface (standard ellipsoid-shaped ROI). (**b**, **b**1) Trabecular bone of M2 (manually drawn ROI delineating the trabecular bone). (**b**, **b**2) Trabecular bone of M2 within the inter-radicular septum (standard ellipsoid-shaped ROI). (**c**, **c**1) Trabecular bone of M3 within the inter-radicular septum (standard ellipsoid-shaped ROI). (**d**, **d**1) Condyle (rectangular-shaped ROI). Cond, condyle; M, molar teeth; ROI, region of interest.

contained between 218 and 230 slices (Figure 3b, b1 and b2). The reference slice was set at the middle slice of the data set. Likewise, as performed for M1, the ROI was delineated manually (Mand. ROI. M2) (Figure 4b, b1) as well as by means of an ellipsoid area, both over a volume of 50 slices. The ellipsoid area (Mand. ROI. M2. InterRad) (Figure 4b, b2) here was positioned in between the roots of the molar, such that the edges were not in contact with the periodontal space of the tooth tissues.

Finally, for M3, a data subset was created containing exclusively the M3 region and defined by the top (that is, the slice where the crown of M3 appears) and bottom slice (that is, the slice where the crown of M3 disappears). The data set contained an average of 373–400 slices (Figure 3c, c1 and c2). The reference slice was defined here as the middle slice of the data set. The VOI analysed consisted of 20 slices downwards from the reference slice. For each of these slices, an ellipsoid area (Mand. ROI. M3. InterRad) measuring 0.4 mm × 0.4 mm was positioned in between the roots of M3 as for M2 (Figure 4c, c1).

In addition to the molar region, the condyle of the mandible was also considered for the analysis of its microarchitecture. Likewise, for the other VOIs, a data subset containing the condyle was created. Using Data Viewer, the sample was re-oriented such that the ramus was positioned vertically. All the analyses were performed on the trans-axial images. The reference slice used for the condyle analysis was the slice where the condyle started appearing. The VOI selected for measurement started at the 50th slice from the reference point over a volume containing 100 slices. Two rectangular ROIs (Mand. ROI. Cond) were used within this VOI to assess the trabecular bone microarchitecture, including the porosities of the condylar head (Figure 3d, d1 and d2). The ROIs were then interpolated for all slices. Two separate analyses were performed with the aim of including all of the trabecular bone in the condylar head, as the shape of the condyle differs from the proximal towards the distal region. The first rectangular ROI with dimensions of 0.5 mm× 0.4 mm was projected onto the slices containing the smaller (distal) part of the condyle, while the other rectangular ROI measuring 0.8 mm × 0.5 mm was drawn onto the slices with the larger (proximal) condyle part. The ROIs were positioned in a vertical direction centrally in the condyle, below the subchondral region (Figure 4d, d1).

Trabecular bone quantification

The quantitative evaluation of the trabecular bone tissue was carried out on the microtomographic data sets generated by direct 3D morphometry. The measurement and reporting of morphometric parameters were performed following the guidelines put forth by Bouxsein *et al.*[1] The BV fraction (BV/TV), trabecular thickness (Tb.Th), trabecular separation (Tb.Sp), and trabecular number (Tb.N) were calculated as 3D measurements of trabecular bone mass and its distribution. Furthermore, the trabecular architecture was evaluated by calculating the connectivity of the trabecular network (trabecular bone pattern formation, Tb.Pf), the structure model index (SMI) and total porosity. Low Tb.Pf values reflected better connected trabeculae, whereas high Tb.Pf values indicated disconnected trabecular structures. The SMI values provided information regarding the trabecular shape, which was either rod- (SMI = 3) or plate-like (SMI = 0). It must be noted that SMI must be interpreted carefully, especially in trabecular bone, as it is unavoidably influenced by aberrations due to negative values and in such cases cannot differentiate between distinctive trabecular geometries.[32]

RESULTS

The method described in the present study resulted in defining procedures for the manual delineation of ROIs as well as for predefined areas (ellipsoid/rectangle) of ROIs with appropriate localization based on well-defined landmarks and known bone morphometric parameters.[1] As a case study, the developed micro-CT protocol was applied to analyse the jawbone microarchitecture of female Wistar rats (Table 2). From the values reported in Table 2, one can observe that there is a significant difference in the BV/TV measured by a fixed ellipsoid (inter-radicular septum region of mandibular M2) versus the manually contoured region. The reason for this could be that the inter-radicular septum is a region close to the tooth root. Since tooth roots are surrounded by the periodontal

Table 2 Case study: morphometric indices corresponding to the specific samples ($n = 16$)

Sample	BV/TV/%	Tb.Th/mm	Tb.Sp/mm	Tb.N/(1 mm^{-1})	Tb.Pf/(1 mm^{-1})	SMI	Porosity/%
Max. ROI. M2	69.31 ± 1.85	0.133 ± 0.005	0.085 ± 0.009	5.26 ± 0.17	−7.84 ± 1.72	0.15 ± 0.18	n/a
Max. ROI. Tub	43.79 ± 1.73	0.12 ± 0.004	0.13 ± 0.002	3.41 ± 0.14	2.01 ± 1.94	1.01 ± 0.22	n/a
Mand. ROI. M1	24.82 ± 0.75	0.101 ± 0.003	0.3 ± 0.002	2.45 ± 0.06	−13.06 ± 1.03	−1.53 ± 0.15	n/a
Mand. ROI. M1. Lingual	46.87 ± 1.51	0.14 ± 0.006	0.147 ± 0.005	3.33 ± 0.11	−4.35 ± 0.97	−0.39 ± 0.24	n/a
Mand. ROI. M1. Buccal	42.76 ± 2.34	0.14 ± 0.007	0.15 ± 0.006	3.06 ± 0.08	−2.64 ± 1.15	−0.09 ± 0.21	n/a
Mand. ROI. M2	29.35 ± 0.73	0.11 ± 0.003	0.23 ± 0.005	2.60 ± 0.08	−9.08 ± 1.34	−0.79 ± 0.14	n/a
Mand. ROI. M2. InterRad	82.02 ± 1.9	0.114 ± 0.003	0.063 ± 0.005	7.24 ± 0.24	−8.64 ± 2	−0.1 ± 0.18	n/a
Mand. ROI. M3. InterRad	81.4 ± 2.46	0.15 ± 0.004	0.05 ± 0.003	7.91 ± 0.2	−4.72 ± 1.82	0.32 ± 0.16	n/a
Mand. ROI. Cond	87.39 ± 1.02	0.122 ± 0.005	0.041 ± 0.001	7.15 ± 0.21	−18.08 ± 1.29	−1.68 ± 0.18	12.60 ± 1.02

BV/TV, bone volume fraction; Cond, condyle; InterRad, inter-radicular; M, molar; Mand, mandible; Max, maxilla; ROI, region of interest; SMI, structure model index; Tb.N, trabecular number; Tb.Pf, trabecular bone pattern formation; Tb.Sp, trabecular separation; Tb.Th, trabecular thickness.

ligament, the different mastication forces experienced here could lead to different bone remodelling rates and outcomes.[33]

DISCUSSION

Previously, the analysis of bone morphology and density was performed by conventional histomorphometry. It then paved the way for analysis by DEXA. However, due to the low resolution and the limitation it offers *via* 2D imaging, it was not possible to determine the microstructural parameters of the bone.[34] However, the emergence of micro-CT methods offering the potential to capitalize on the 3D evaluation of the bone structural parameters holds promise. It also avoids variability by observers and accounts for the variation of bone parameters within a particular sample. The use of micro-CT imaging to assess the trabecular and cortical bone structure in animals and humans has increased exponentially. There are several commercially available micro-CT systems leading to various image acquisition approaches, image evaluation, and reporting of outcomes. However, the majority of the experimental reports lack details of the protocol applied for micro-CT image analysis. In particular, protocols aimed at quantifying the rodent jawbone have been poorly described and lack information, thereby impeding or even excluding the generation of the replicate data.[21] Currently, there are 17 different micro-CT software programmes that are used for the quantification of the rodent jawbone architecture[21] leading to a large variability of analytical methods between the studies. Image acquisition and processing, especially segmentation and filtration due to the different software programmes, were often not clearly explained.[1] The size and location of ROIs also differed between the groups and were not standardized. In some studies, the ROIs used were not scaled to the dimensions of the bone size, causing inaccurate measurements of the trabecular bone and resulting in over-sampling between the compared studies.[23] This eventually leads to discrepancies and inconsistency in reporting the results. This lack of consistency makes it very difficult to interpret the reported outcomes and to compare the findings across the different studies. Thus, there is a need to use standardized terminologies and report the parameters evaluated, particularly with respect to micro-CT analysis of rodent specimens.[1,21] Precise protocols are in particularly mandatory for analysing the significance of the outcome of the results. Moreover, the results can be biased if the procedures are not standardized, as the system is extremely user-sensitive. Thus, the present paper proposes a methodology for standardized, accurate, and reproducible quantitative analysis of the rat jawbone microarchitecture using micro-CT imaging. It primarily focuses on the standardization of the procedures for evaluating trabecular bone in the rat jaw using both manual and semi-automatic delineation as well as the appropriate positioning of the volumes of interest to be analysed.

The main purpose was to define a robust protocol for the rodent jawbone based on the guidelines established by Bouxsein *et al.*[1] Although in general, specific experiments and research questions dictate the protocol, it is important to follow a uniform system of reporting of all the steps involved in the micro-CT measurements right from the steps of image acquisition up to the quantitative analysis and reporting of results.

Some important considerations to keep in mind while quantifying rodent jawbones are summarized as follows. (i) With regard to image acquisition, as the rat jawbone is particularly challenging in terms of the small size of the bones and structures of interest, such as the trabecular bone, it is important to produce high-quality images. The choice of voxel size is critical in order to make reliable measurements. Ideally, the smallest voxel size (highest scan resolution) is used for scanning; however, this results in longer acquisition times, as they need to collect more projections and create large data sets. Thus, an appropriate trade-off between voxel size and scanning time should be taken into account. Differences between 10 and 20 μm will not have a huge impact on the structures that have large thicknesses (100–200 μm). However, when evaluating smaller trabecular structures in the mouse and rat with approximate dimensions between 20 and 60 μm, such differences can have a huge impact due to underestimation of the bone mineral density (due to partial volume effects) and overestimation of the object thickness. In such scenarios, the ratio of the voxels to object size is important, as the higher the ratio, the more accurate the morphologic measurements.[1] It is also very important to maintain an optimal ratio between the pixel size and the size of the sample visualized. This ensures that high-resolution imaging can be achieved through higher photon counts, thereby reducing time costs, which should not exceed the ratio of 1:4. The *ex vivo* micro-CT applied in the present study has a voxel size of 7.69 μm^3, which is high enough to achieve accurate measurements quite comfortably. (ii) With regard to imaging analysis, the scanned images should be visually inspected for significant artefacts, such as ring or motion artefacts, before applying 3D algorithms to quantify the trabecular bone structure. In the current protocol, the ring reduction was set at 15 to remove artefacts caused by the scanning. (iii) Image filtration should be applied to reduce signal noise and maintain sharp contrast between the bone and the marrow areas. Gaussian filtering using appropriate thresholding should be adopted to remove image noise. (iv) Image segmentation is critical in separating the mineralized and non-mineralized tissues for quantitative analysis. It is of utmost importance to compare the images of the original with the segmented ones to ensure that the extracted bone is representative of the original structure, as any error will systematically impact the results. The protocol applied in the present case study made use of global

thresholding, which employs a fixed range of greyscales (lower and upper scales set at 70 and 224) for both foreground (white) and the pixels outside of the range area, which are set as the background (black). There are also other thresholding options available, such as adaptive, automatic, and multilevel thresholding; however, in the current protocol, since the region of interest comprises trabecular bone, the global thresholding option is able to achieve the desired image filtration. Finally, (v) selecting the appropriate VOI at a particular site is essential. The contouring method used for the delineation of the bone can either be automatic (as proposed in upgrades of the Skyscan software), a self-defined fixed ellipsoid or rectangular area that captures the bone of interest or an ROI with an irregular contour drawn manually on a slice-by-slice method. Applying a regular, uniformly shaped ROI could include spaces devoid of bone, thereby reducing the values of BV/TV at that region and leading to the masking of relevant differences between the experimental groups. For example, in the current methodology, the suture-forming elements between the maxilla and sphenoid as well as the mandibular canal (the regular circular opening in the ROI of most jawed species) is omitted during the analysis of the trabecular bone. This is because the sutures of the maxilla are not connected by bone and the mandibular canal contains a neuro-vascular bundle enclosed around a compact bone shell, which is devoid of trabecular bone. Such considerations are very valuable to keep in mind during analysis, as it demonstrates the importance of the VOI selection and the risk of sampling across several adjacent bones. Thus, depending on the anatomic skeletal site of interest, the appropriate type of contouring method can be selected. Since some of the trabecular parameters are influenced by changes in VOI size and location, caution must be taken when interpreting the significant differences between the different trabecular parameters. Thus, it is recommended that researchers try to understand the existing biases in their studies by testing the effect of different VOI sizes and location to accurately interpret the functional differences of trabecular parameters. The choice of VOI size and location should be guided by an understanding of the function of the bone (for example, loading) and the anatomical region in different species. Trabecular analyses of irregularly shaped bones are often constricted by anatomy, and in these cases, it is often better to determine biomechanically rather than anatomically homologous VOIs.[35] The choice of VOI size and location should be guided by an understanding of the function of the bone (for example, loading) and the anatomical region in different species.

A limitation encountered while formulating the protocol involved the extraction of the cortical bone in the rodent jaw. The cortical bone was difficult to visualize due to its similarity in grey values with the dentin and enamel in the jawbone. One way to measure the cortical bone was to include the whole mandible or maxilla, subsequently exclude the teeth, and then deduct the trabecular region that was measured earlier in the molar region. However, this proved to be difficult to implement due to the extraction of the teeth and roots in the molar region and the presence of the sinus and nasal cavities in the maxilla. The excision of irregularly shaped bones of the teeth and their roots from the image of interest proved to be arduous. It made it very challenging to acquire a standard and reproducibly shaped VOI for all specimens to be analysed and to obtain a consistent shape between the different animals. These difficulties in measurements may explain the lack of studies that consistently quantify cortical bone changes in the rodent jaw.[36] Opting for higher resolution of images with nano-computed tomography (nano-CT) with the use of contrast agents could help in providing the necessary contrast in visualization between bone and dentin and the quantification of cortical bone in an accurate manner. Nevertheless, micro-CT and nano-CT cannot be used in a clinical setting to measure the structural parameters of the bone, and this is where cone beam computed tomography (CBCT) can help. However, it must be duly noted that CBCT has a lower spatial resolution and can only measure structures that lie within the voxel size of 76 and 300 μm.[37] Since in our current protocol, the visualized trabecular structures are much below the resolution range of the CBCT, micro-CT is a better option. Another preferred choice for image quantification is *in vivo* micro-CT. It can monitor bone changes that occur in real time over a period of several months. It also has the possibility to employ radiopaque contrast agents, which can enhance image visibility in different conditions, such as micro damage,[38] vascular morphology,[39–42] and cartilage degradation.[43–44] Nonetheless, this type of CT also has its own issues with regard to the dosage of radiation supplied, which can prove to be harmful if the specimen is monitored over a long period of time, along with movement artefacts that the images encounter during image acquisition.[1] Thus, depending on the research question and the experiment performed, any of the above imaging techniques can be used.

Even though the current study focuses mainly on the *ex vivo* evaluation of the rodent jawbone using desktop micro-CT systems, these guidelines can be adjusted and applied to a wide range of protocols in other species' jawbones as well. Moreover, the key outcome of this study is the establishment of a method that is able to define the VOI in the rodent jawbone in a standardized and reproducible manner for the evaluation of trabecular bone morphology.

CONCLUSION

Ultimately, the protocol developed in this work provides a robust and reproducible methodology for micro-CT analysis of relevant rat jawbone ROIs and is intended to ensure the global, accurate, and consistent reporting of micro-CT-derived jawbone morphometry. By including various ROIs most susceptible to bone changes as a result of experimental interventions within the jawbone, one can have a wide range of ROIs to choose from, depending on the experimental study. The protocol is straightforward and can be adapted to any micro-CT software associated with the different commercial systems available. Finally, the proposed methodology has potential, as a variety of rodent animal models would benefit from its implementation.

ACKNOWLEDGEMENTS

This study was funded by the Fund for Scientific Research—Flanders (FWO) (G.0726.09). This work was further supported by postdoctoral researcher C Correa (2014/0892-1), University of Campinas, Brazil and (245450/2012-2) postdoctoral researcher F Faot, Federal University of Pelotas, Brazil.

1 Bouxsein ML, Boyd SK, Christiansen BA *et al.* Guidelines for assessment of bone microstructure in rodents using micro-computed tomography. *J Bone Miner Res* 2010; **25**(7): 1468–1486.
2 Parfitt AM, Drezner MK, Glorieux FH *et al.* Bone histomorphometry: standardization of nomenclature, symbols, and units. Report of the ASBMR Histomorphometry Nomenclature Committee. *J Bone Miner Res* 1987; **2**(6): 595–610.
3 Gielkens PF, Schortinghuis J, De Jong JR *et al.* A comparison of micro-CT, microradiography and histomorphometry in bone research. *Arch Oral Biol* 2008; **53**(6): 558–566.
4 Müller R, Van Campenhout H, Van Damme B *et al.* Morphometric analysis of human bone biopsies: a quantitative structural comparison of histological sections and micro-computed tomography. *Bone* 1998; **23**(1): 59–66.
5 Rhee Y, Hur JH, Won YY *et al.* Assessment of bone quality using finite element analysis based upon micro-CT images. *Clin Orthop Surg* 2009; **1**(1): 40–47.
6 Müller R. Hierarchical microimaging of bone structure and function. *Nat Rev Rheumatol* 2009; **5**(7): 373–381.

7 Feldkamp LA, Goldstein SA, Parfitt AM *et al.* The direct examination of three-dimensional bone architecture *in vitro* by computed tomography. *J Bone Miner Res* 1989; **4**(1): 3–11.
8 Kallai I, Mizrahi O, Tawackoli W *et al.* Microcomputed tomography-based structural analysis of various bone tissue regeneration models. *Nat Protoc* 2011; **6**(1): 105–110.
9 Dai QG, Zhang P, Wu YQ *et al.* Ovariectomy induces osteoporosis in the maxillary alveolar bone: an *in vivo* micro-CT and histomorphometric analysis in rats. *Oral Dis* 2014; **20**(5): 514–520.
10 Kuroshima S, Kovacic BL, Kozloff KM *et al.* Intra-oral PTH administration promotes tooth extraction socket healing. *J Dent Res* 2013; **92** (6): 553–559.
11 Xu YQ, Zhao TM, Xu WJ *et al.* Periodontal microstructure change and tooth movement pattern under different force magnitudes in ovariectomized rats: an *in-vivo* microcomputed tomography study. *Am J Orthod Dentofacial Orthop* 2013; **143**(6): 828–836.
12 Abtahi J, Agholme F, Sandberg O *et al.* Effect of local *vs.* systemic bisphosphonate delivery on dental implant fixation in a model of osteonecrosis of the jaw. *J Dent Res* 2013; **92**(3): 279–283.
13 Alikhani M, Khoo E, Alyami B *et al.* Osteogenic effect of high-frequency acceleration on alveolar bone. *J Dent Res* 2012; **91**(4): 413–419.
14 Bagi CM, Berryman E, Moalli MR. Comparative bone anatomy of commonly used laboratory animals: implications for drug discovery. *Comp Med* 2011; **61**(1): 76–85.
15 Kosugi K, Yonezu H, Kawashima S *et al.* A longitudinal study of the effect of experimental osteoporosis on bone trabecular structure in the rat mandibular condyle. *Cranio* 2013; **31**(2): 140–150.
16 Mijares D, Kulkarni A, Lewis K *et al.* Oral bone loss induced by mineral deficiency in a rat model: effect of a synthetic bone mineral (SBM) preparation. *Arch Oral Biol* 2012; **57**(9): 1264–1273.
17 Ravosa MJ, Klopp EB, Pinchoff J *et al.* Plasticity of mandibular biomineralization in myostatin-deficient mice. *J Morphol* 2007; **268**(3): 275–282.
18 Shimizu Y, Ishida T, Hosomichi J *et al.* Soft diet causes greater alveolar osteopenia in the mandible than in the maxilla. *Arch Oral Biol* 2013; **58**(8): 907–911.
19 Tanaka M, Miyazawa K, Tabuchi M *et al.* Effect of reveromycin a on experimental tooth movement in OPG-/- mice. *J Dent Res* 2012; **91**(8): 771–776.
20 Chang PC, Chung MC, Wang YP *et al.* Patterns of diabetic periodontal wound repair: a study using micro-computed tomography and immunohistochemistry. *J Periodontol* 2012; **83**(5): 644–652.
21 Faot F, Chatterjee M, de Camargos GV *et al.* Micro-CT analysis of the rodent jaw bone micro-architecture: a systematic review. *Bone Rep* 2015; **2**: 14–24.
22 Kivell TL, Skinner MM, Lazenby R *et al.* Methodological considerations for analyzing trabecular architecture: an example from the primate hand. *J Anat* 2011; **218**(2): 209–225.
23 Lazenby RA, Skinner MM, Kivell TL *et al.* Scaling VOI size in 3D μCT studies of trabecular bone: a test of the over-sampling hypothesis. *Am J Phys Anthropol* 2011; **144**(2): 196–203.
24 Whitehouse WJ, Dyson ED. Scanning electron microscope studies of trabecular bone in the proximal end of the human femur. *J Anat* 1974; **118**(Pt 3): 417–444.
25 Berglundh T, Stavropoulos A, Working Group 1 of the VIII European Workshop on Periodontology. Preclinical *in vivo* research in implant dentistry. Consensus of the eighth European workshop on periodontology. *J Clin Periodontol* 2012; **39**(Suppl 12): 1–5.
26 Kilkenny C, Browne WJ, Cuthill IC *et al.* Improving bioscience research reporting: the ARRIVE guidelines for reporting animal research. *PLoS Biol* 2010; **8**(6): e1000412.
27 Mavropoulos A, Rizzoli R, Ammann P. Different responsiveness of alveolar and tibial bone to bone loss stimuli. *J Bone Miner Res* 2007; **22**(3): 403–410.
28 Prado RF, Silveira VÁ, Rocha RF *et al.* Effects of experimental osteoporosis and low calcium intake on postextraction sockets of rats. *Int J Exp Pathol* 2012; **93**(2): 139–147.
29 Yang J, Pham SM, Crabbe DL. Effects of oestrogen deficiency on rat mandibular and tibial microarchitecture. *Dentomaxillofac Radiol* 2003; **32**(4): 247–251.
30 Ejiri S, Tanaka M, Watanabe N *et al.* Estrogen deficiency and its effect on the jaw bones. *J Bone Miner Metab* 2008; **26**(5): 409–415.
31 Mavropoulos A, Kiliaridis S, Rizzoli R *et al.* Normal masticatory function partially protects the rat mandibular bone from estrogen-deficiency induced osteoporosis. *J Biomech* 2014; **47**(11): 2666–2671.
32 Salmon PL, Ohlsson C, Shefelbine SJ *et al.* Structure model index does not measure rods and plates in trabecular bone. *Front Endocrinol* 2015; **6**: 162.
33 Hsu PY, Tsai MT, Wang SP *et al.* Cortical bone morphological and trabecular bone microarchitectural changes in the mandible and femoral neck of ovariectomized rats. *PLoS One* 2016; **11**(4): e0154367.
34 Kuroda S, Mukohyama H, Kondo H *et al.* Bone mineral density of the mandible in ovariectomized rats: analyses using dual energy X-ray absorptiometry and peripheral quantitative computed tomography. *Oral Dis* 2003; **9**(1): 24–28.
35 Maga M, Kappelman J, Ryan TM *et al.* Preliminary observations on the calcaneal trabecular microarchitecture of extant large-bodied hominoids. *Am J Phys Anthropol* 2006; **129**(3): 410–417.
36 Westerlind KC, Wronski TJ, Ritman EL *et al.* Estrogen regulates the rate of bone turnover but bone balance in ovariectomized rats is modulated by prevailing mechanical strain. *Proc Natl Acad Sci USA* 1997; **94**(8): 4199–4204.
37 Van Dessel J, Huang Y, Depypere M *et al.* A comparative evaluation of cone beam CT and micro-CT on trabecular bone structures in the human mandible. *Dentomaxillofac Radiol* 2013; **42**(8): 20130145.
38 Leng HJ, Wang X, Ross RD *et al.* Micro-computed tomography of fatigue microdamage in cortical bone using a barium sulfate contrast agent. *J Mech Behav Biomed Mater* 2008; **1**(1): 68–75.
39 Duvall CL, Taylor WR, Weiss D *et al.* Impaired angiogenesis, early callus formation, and late stage remodeling in fracture healing of osteopontin-deficient mice. *J Bone Miner Res* 2007; **22**(2): 286–297.
40 Chen RR, Snow JK, Palmer JP *et al.* Host immune competence and local ischemia affects the functionality of engineered vasculature. *Microcirculation* 2007; **14**(2): 77–88.
41 Duvall CL, Taylor WR, Weiss D *et al.* Quantitative microcomputed tomography analysis of collateral vessel development after ischemic injury. *Am J Physiol Heart Circ Physiol* 2004; **287**(1): H302–H310.
42 Duvall CL, Weiss D, Robinson ST *et al.* The role of osteopontin in recovery from hind limb ischemia. *Arterioscler Thromb Vasc Biol* 2008; **28**(2): 290–295.
43 Palmer AW, Guldberg RE, Levenston ME. Analysis of cartilage matrix fixed charge density and three-dimensional morphology *via* contrast-enhanced microcomputed tomography. *Proc Natl Acad Sci USA* 2006; **103**(51): 19255–19260.
44 Xie L, Lin AS, Levenston ME *et al.* Quantitative assessment of articular cartilage morphology *via* EPIC-microCT. *Osteoarthritis Cartilage* 2009; **17**(3): 313–320.